

Viscoelastic flow simulation of polytetrafluoroethylene (PTFE) paste extrusion

Pramod D. Patil, Isaias Ochoa, James J. Feng, Savvas G. Hatzikiriakos*

Department of Chemical and Biological Engineering, The University of British Columbia, 2360 East Mall, Vancouver, BC V6T 1Z3, Canada

Received 9 September 2007; received in revised form 7 November 2007; accepted 17 November 2007

Abstract

Polytetrafluoroethylene (PTFE) is known to be a polymer that shows inherent microstructure formation during cold processing such as paste extrusion. To model such a complex flow, a viscoelastic constitutive equation is proposed that takes into account the continuous change of the paste microstructure during flow, through fibril formation. The mechanism of fibrillation is captured through a microscopic model for a structural parameter ξ that represents the percentage of fibrillated domains of the paste. The proposed viscoelastic constitutive equation consists of a viscous shear-thinning term (Carreau model) and an elastic term (modified Mooney–Rivlin model), the relative contribution of the two depending on ξ . The viscous and elastic parameters of the model are determined by using shear and extensional rheometry on the paste. Finite element simulations based on the proposed constitutive relation with the measured model parameters predict reasonably well the variations of the extrusion pressure with the apparent shear rate and the die geometrical characteristics.

© 2007 Elsevier B.V. All rights reserved.

Keywords: Fibrillation; Structural parameter; Flow type parameter; Viscoelasticity; Strain-hardening; Finite element simulations; Hyperelasticity

1. Introduction

Polytetrafluoroethylene (PTFE) paste is a mixture of PTFE particles of submicron primary size (typically 0.20–0.25 μm) with an isoparaffinic lubricant at 0.16–0.22 wt.%. During its flow, structural changes occur that significantly influence its rheology [1–6]. The most remarkable feature is the formation of fibrils between neighboring polymer particles. It is these fibrils of submicron size in diameter that essentially give the dimensional stability and strength to the final extruded product.

The die geometry shown in Fig. 1 is typically used in the rod extrusion of PTFE paste. The main geometrical characteristics are the entry angle 2α , the reduction ratio RR, defined as the ratio of the initial to the final cross-sectional area of the conical entry $RR \equiv D_0^2/D^2$, and the length-to-diameter ratio of the die land L/D .

A significant, counterintuitive experimental observation is that the extrusion pressure, p , varies non-monotonically with the entrance angle of the conical die 2α ; it attains a minimum

at an entrance angle, $2\alpha \approx 30\text{--}40^\circ$. Patil et al. [5] surmised that the unusual dependence of extrusion pressure p on 2α is due to the continuous microfibril formation that changes the nature of the fluid from a shear thinning fluid-like behavior to a solid-like elastic one [5]. However, they have proposed an ad hoc constitutive equation that accounts for the increase in fibrillation at high entrance angles through a shear-thickening viscosity. This approach has two weaknesses: (i) the rheological consequence of fibrillation should be of elastic and not of viscous (shear-thickening) origin, and (ii) the parameters of the proposed constitutive model are treated as adjustable to a large extent, and cannot be directly related to measured rheological properties of the paste. The present study aims to remove both shortcomings.

First, we propose a viscoelastic constitutive equation based on the concept of a structural parameter, ξ , which is described by a first-order kinetic differential equation [5]. This parameter represents the percentage of the domains (sets of particles) of the PTFE material that are fibrillated and takes values of 0 and 1 for the unfibrillated and fully fibrillated (all particles interconnected with fibrils into a network) cases, respectively. The total stress tensor consists of a viscous part modeled by the shear-thinning Carreau equation, and an elastic part given by a modified Mooney–Rivlin model. The latter is borrowed from

* Corresponding author. Tel.: +1 604 822 3107; fax: +1 604 822 6003.
E-mail address: hatzikir@interchange.ubc.ca (S.G. Hatzikiriakos).

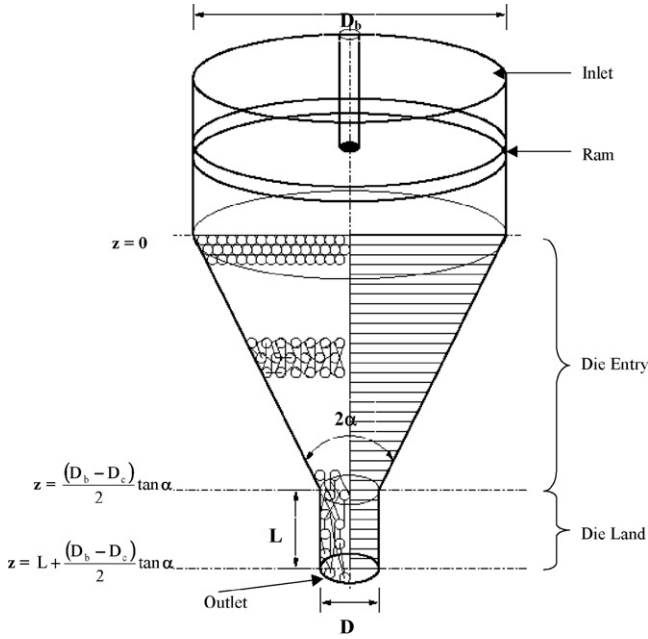


Fig. 1. A conical entry die used in the paste extrusion of PTFE: the left half illustrates the extrusion of PTFE particles and the gradual structure formation through particle fibrillation, whereas the shaded area depicts the axisymmetric domain used in the simulations (reproduced from Patil et al. [5]).

hyperelastic modeling of rubbers [7–11]. The relative contribution of the two depends on ξ .

The model parameters in the constitutive equation are determined from independent rheological measurements using a parallel-plate and an extensional rheometer. The paste before processing shows shear thinning fluid-like behavior with no fibrillation, which is characterized by simple shear experiments. The paste after processing shows strain hardening behavior with significant amount of fibrillation, which is characterized by extension rheometry. This removes the second shortcoming of the model proposed by Patil et al. [5].

The viscoelastic constitutive equation with model parameters determined by independent rheological experiments are subsequently used to simulate the flow of pastes through the conical die depicted in Fig. 1. The finite element results are used to predict the extrusion pressure as a function of the operating and die geometrical characteristics. Finally, we compare the flow simulation results with experimental measurements such as the pressure drop as a function of the apparent shear rate and geometric characteristics of the die. The results are also compared with the results presented by Patil et al. [5].

2. Theoretical modeling and numerical method

2.1. Governing equations

For steady incompressible flow, the balance of mass and momentum becomes (volume changes due to fibril formation are assumed to be small):

$$\nabla \cdot \mathbf{v} = 0, \quad (1)$$

$$\nabla p - \nabla \cdot \boldsymbol{\tau} = 0, \quad (2)$$

where p is the pressure and $\boldsymbol{\tau}$ is the stress tensor, which depends on the structural parameter ξ through a viscoelastic constitutive equation discussed below. Due to the high viscosity of the paste, inertia is neglected in the momentum equation (Eq. (2)). To simulate the flow of the PTFE paste, the above equations are coupled with the rheological constitutive model. The axisymmetric r - z domain (Fig. 1) has been used to perform the simulations.

2.1.1. Constitutive equation

To model the complex flow behavior of PTFE paste, a constitutive equation is proposed which explicitly accounts for the evolution of fibrils and its effect on paste rheology. Similar approach has been adopted before to model the behavior of concentrated suspensions, polymer solutions and filled polymers [12,13]. While the paste initially behaves as a shear-thinning fluid, after the appearance of fibrils in its structure, it behaves more and more as an elastic solid-like body. Thus, it is assumed that the stress tensor consists of two contributions coming from the unfibrillated and fibrillated domains of the paste, represented by a shear-thinning viscous stress and an elastic stress component respectively. The relative significance of the two contributions depends on the structural parameter ξ [5], the volume percentage of fibrillated domains:

$$\boldsymbol{\tau} = (1 - \xi)\eta_1 \dot{\boldsymbol{\gamma}} + \xi \boldsymbol{\tau}_E, \quad (3)$$

where $\dot{\boldsymbol{\gamma}}$ is the rate of strain tensor, and η_1 is a shear-thinning viscosity that is expressed by a Carreau model [12]:

$$\eta_1 = \eta_{01} [1 + (\alpha_1 \dot{\boldsymbol{\gamma}})^2]^{(n_1 - 1)/2}, \quad (4)$$

$\dot{\boldsymbol{\gamma}}$ being the second invariant of strain rate tensor $\dot{\boldsymbol{\gamma}}$. The term $\boldsymbol{\tau}_E$ denotes the elastic stress due to the fibrillated domains. To select a model for the elastic stress $\boldsymbol{\tau}_E$, we follow the approach used in hyperelasticity [7–11]. When a solid body is subjected to a large deformation, the relationship of positions in deformed and undeformed configurations is described by a deformation gradient tensor \mathbf{F} whose eigenvalues λ_1 , λ_2 , and λ_3 are the stretching ratios in the principal directions. The Mooney–Rivlin equation relates the Cauchy stress tensor $\boldsymbol{\tau}_E$ to the Cauchy–Green strain tensor $\mathbf{B} = \mathbf{F}\mathbf{F}^T$ by

$$\boldsymbol{\tau}_E = 2 \frac{\partial W}{\partial I_1} \mathbf{B} - 2 \frac{\partial W}{\partial I_2} \mathbf{B}^{-1}, \quad (5)$$

where the strain energy density function W is a function of the strain invariants [8,9]:

$$W = W(I_1, I_2, I_3), \quad I_1 = \text{tr} \mathbf{B}, \\ I_2 = \frac{1}{2} \{(\text{tr} \mathbf{B})^2 - \text{tr}(\mathbf{B}\mathbf{B})\}, \quad I_3 = \det \mathbf{B}. \quad (6)$$

Since the PTFE paste can be assumed to be incompressible, the value of I_3 is taken to be unity. Thus, the description of W as a function of I_1 and I_2 forms the basis of our approach. Alternatively, on the basis of the Valanis–Landel hypothesis [14], W can also be expressed directly as a function of the three principal stretches λ_1 , λ_2 , and λ_3 . To capture the rate dependent response

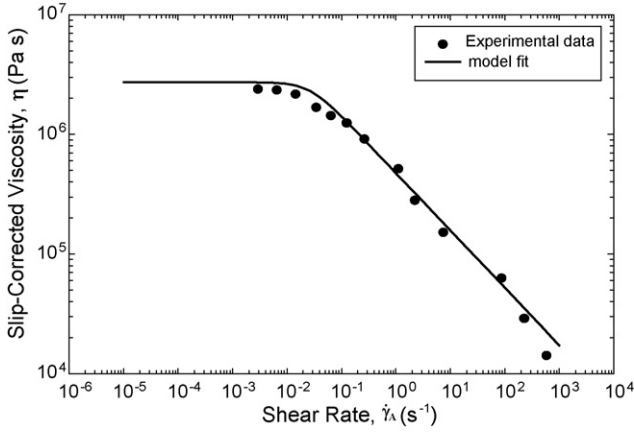


Fig. 2. The corrected viscosity of the sample F104 HMW fitted using the Carreau model in Eq. (4). The parameter values are listed in Table 3.

of hyperelastic materials, W should also depend on the strain rate $\dot{\gamma}$ [11]:

$$W = W(\dot{\gamma}, I_1, I_2). \quad (7)$$

In the present study, we use the following form of the strain energy function:

$$W(I_1, I_2) = C_1(I_1 - 3) + C_2 \ln\left(\frac{\dot{\gamma}}{\dot{\gamma}_c}\right) (I_1 - 3)^n + C_3 \ln\left(\frac{\dot{\gamma}}{\dot{\gamma}_c}\right) (I_1 - 3)^m + C_4(I_2 - 3), \quad (8)$$

where $C_1, C_2, C_3, C_4, n,$ and m are material parameters, and $\dot{\gamma}_c$ is a threshold strain-rate below which rate-dependence is absent ($C_2 = C_3 = 0$ for $\dot{\gamma} < \dot{\gamma}_c$). Eq. (8) embodies ideas from both Selvadurai and Yu [11] and Amin et al. [10]. The power-law terms come from Amin et al. [10]. The C_2 term, with $C_2 > 0$, predicts the hardening feature observed at higher strain levels [10,15,16]. Similarly, the C_3 term, with $C_3 < 0$, accounts for the initial stiffness encountered in elastic materials [10]. The log-factors that incorporate rate-dependence are borrowed from Selvadurai and Yu [11].

Let us consider the predictions of Eq. (8) in steady uniaxial elongation, with principal stretch ratio (λ_1) in the loading direction and compression in the other two directions with $\lambda_2 = \lambda_3 = \lambda_1^{-1/2}$ owing to isotropy and incompressibility. The deformation gradient tensor \mathbf{F} and Cauchy–Green deformation tensor \mathbf{B} can be written as

$$\mathbf{F} = \begin{pmatrix} \lambda_1 & 0 & 0 \\ 0 & \sqrt{\frac{1}{\lambda_1}} & 0 \\ 0 & 0 & \sqrt{\frac{1}{\lambda_1}} \end{pmatrix}, \quad \mathbf{B} = \begin{pmatrix} \lambda_1^2 & 0 & 0 \\ 0 & \frac{1}{\lambda_1} & 0 \\ 0 & 0 & \frac{1}{\lambda_1} \end{pmatrix}, \quad (9)$$

and the strain invariants as

$$I_1 = \frac{2}{\lambda_1} + \lambda_1^2, \quad I_2 = \frac{1}{\lambda_1^2} + 2\lambda_1, \quad I_3 = 1, \quad (10)$$

Table 1

Physical properties of PTFE fine powder resin studied in this work as provided by the supplier

Resin	Type	Particle diameter (μm)	Specific gravity
F104 HMW	Homopolymer	400–650	2.17–2.20
F104 LMW	Homopolymer	400–650	2.16–2.18
F301	Modified	400–650	2.15–2.18
F303	Modified	400–700	2.14–2.16

where $\lambda_1 = L/L_0$, L_0 being the original length of the sample and L being the length of the deformed sample. Using Eqs. (5) and (8), the expression for the tensile stress component $\tau_{E,11}$ can be written as [10,17]:

$$\tau_{E,11} = 2 \left(\lambda_1^2 - \frac{1}{\lambda_1} \right) \left(\frac{\partial W}{\partial I_1} + \frac{1}{\lambda_1} \frac{\partial W}{\partial I_2} \right). \quad (11)$$

Using Eq. (8), the Eq. (11) can be written as

$$\tau_{E,11} = 2 \left(\lambda_1^2 - \frac{1}{\lambda_1} \right) \left[C_1 + C_2 \ln\left(\frac{\dot{\gamma}}{\dot{\gamma}_c}\right) \left(\frac{2}{\lambda_1} + \lambda_1^2 - 3 \right)^n + C_3 \ln\left(\frac{\dot{\gamma}}{\dot{\gamma}_c}\right) \left(\frac{2}{\lambda_1} + \lambda_1^2 - 3 \right)^m + \frac{C_4}{\lambda_1} \right]. \quad (12)$$

By measuring experimentally the tensile stress as a function of strain at various strain rates, the parameters C_1, C_2, C_3, C_4, m and n can be determined by fitting experimental data to Eq. (12).

2.1.2. Experimental analysis and parameter estimation

To obtain the values of the viscous parameters η_{01}, n_1 and α_1 , steady shear experiments were performed using a stress-controlled rheometer equipped with parallel plates geometry (C-VOR Bohlin). The samples were prepared using various PTFE resins and an isoparaffinic lubricant Isopar[®] M. The physical properties of PTFE resins and the lubricant (ISOPAR[®] M) are listed in Tables 1 and 2, respectively. The paste was first compacted and shaped into discs before being loaded onto the rheometer. Sand paper was glued onto the plates to suppress slippage. To estimate the slip-corrected rheological data, the experiments were performed for two different gap sizes of 1.0 and 2.1 mm at room temperature, with stress values ranging from 100 to 4000 Pa.

Due to the use of sand paper, no slip occurs at low shear stress values. However, significant slip was observed at higher stress values. Assuming that the slip velocity depends only on the shear stress σ_w , Yoshimura and Prud'Homme [18] suggested

Table 2

Physical properties of the Isopar[®] M lubricant used in the PTFE paste extrusion experiments

Property	Isopar [®] M
Density ($\text{g/cm}^3, 25^\circ\text{C}$)	0.79
Surface tension ($\text{dynes/cm}, 25^\circ\text{C}$)	26.6
Vapour pressure ($\text{mmHg}, 38^\circ\text{C}$)	3.1
Viscosity ($\text{mPa s}, 25^\circ\text{C}$)	2.70

Table 3

Parameter values for the shear-thinning model of Eq. (4) fitted to the viscosity function of the paste of F104 HMW with the lubricant Isopar[®] M

Parameters	Shear-thinning
η_0 (Pa s)	2.73×10^6
α_1 (s)	38.13
n	0.52

the following relation for correcting the strain rate and viscosity:

$$\dot{\gamma}_R(\sigma_w) = \frac{H_1 \dot{\gamma}_{a1}(\sigma_w) - H_2 \dot{\gamma}_{a2}(\sigma_w)}{H_1 - H_2}, \quad (13)$$

and

$$\eta(\dot{\gamma}_R) = \frac{\sigma_w(H_1 - H_2)}{H_1 \dot{\gamma}_{a1}(\sigma_w) - H_2 \dot{\gamma}_{a2}(\sigma_w)}, \quad (14)$$

where $\dot{\gamma}_R$ is the corrected shear rate, and $\dot{\gamma}_{a1}$ and $\dot{\gamma}_{a2}$ are the apparent shear rates corresponding to gap sizes of H_1 and H_2 . Fig. 2 plots the slip-corrected viscosity as a function of shear rate. These data are used to determine the viscous parameters in Eq. (4). The best-fit parameters are listed in Table 3, and the corresponding viscosity function is also plotted in Fig. 2.

To determine the parameters of the proposed hyperelastic model, Eq. (12) can be fitted to measured elongational properties of extruded PTFE paste [19]. The uniaxial extension experiments are performed on four different pastes with F104 HMW-Isopar[®] M, F104 LMW-Isopar[®] M, F301-Isopar[®] M and F303-Isopar[®] M at 38.8 vol.% of lubricant. The samples were prepared by extruding the pastes through a slit die (for more details see Ochoa [19]) to produce rectangular-shaped samples. The extruded samples are assumed to be fully fibrillated ($\xi \approx 1$) and thus viscous contribution to their rheological response is assumed to be negligible. The prepared rectangular samples were loaded onto the Sentmanat Extensional Rheometer (SER) attached to a strain-controlled rheometer [20], and were stretched at constant Hencky strain rates in the range of 0.00113 – 1.13 s^{-1} . Table 4 lists the parameter values determined for the four pastes.

For F104HMW, F104LMW and F301, Eq. (12) represents the experimental data reasonably well as can be seen in Fig. 3a–c. However, in the case of resin F303 (co-polymer), which displays a lower extensibility than the other pastes, Eq. (12) does not describe the data very well due perhaps to early yielding (see Fig. 3d). The numerical simulations and comparison with experiments will be carried out for F104HMW for the sake of simplicity. Similar results can be obtained for F104LMW and F301 resins.

Table 4

Model parameters obtained by fitting Eq. (12) to extensional measurements of PTFE samples subjected to different Hencky strain rates (see Figs 5 and 6)

Resin	C_1	C_2	N	C_3	C_4	M	$\dot{\gamma}_c$
F104 HMW	7.66	2.56	0.81	−9.98	4.4	0.135	1.36×10^{-5}
F104 LMW	12.30	4.8	1.10	−11.70	7.22	0.087	1.36×10^{-5}
F301	8.10	18.8	0.69	−7.30	3.66	0.052	1.36×10^{-5}
F303	0.014	25	0.26	−14.10	0.38	0.23	1.36×10^{-5}

2.1.3. Structural parameter

The kinetic model for the structural parameter, ξ , previously proposed in Ref. [5] is also used here. The variation of ξ along a streamlines is determined by the rates of fibril creation and breakage:

$$\mathbf{v} \cdot \nabla \xi = \dot{\gamma} \sqrt{\psi} - \dot{\gamma} \xi, \quad (15)$$

where ψ is the flow type parameter, and $\dot{\gamma}$ is the magnitude of the strain rate tensor. With $\xi=0$ at the inlet of the die, ξ is subsequently bounded between 0 and 1 if $\alpha/\beta \leq 1$. In this study, the creation and evolution of fibrils is due to elongational flow [5,21]. This is reflected by making the rate of creation to depend on the flow type parameter, ψ , which indicates the relative strength of straining and rotation in a mixed flow [13,22,23]. More details about this model can be found in Patil et al. [5].

2.2. Boundary conditions

For the various boundary segments in the axisymmetric geometry shown in Fig. 1 the following boundary conditions are used:

- (i) *Inlet boundary conditions* ($z=0$). The fully developed velocity profile for a shear-thinning Carreau fluid model has been imposed at the inlet with radial velocity $v_r = 0$. The paste is completely unfibrillated at this point: $\xi = 0$. In addition, the initial strain is set to zero:

$$\mathbf{F} = \begin{pmatrix} 1 & 0 & 0 \\ 0 & 1 & 0 \\ 0 & 0 & 1 \end{pmatrix}.$$

Due to wall slip, the strain of the upstream shear is small, and thus negligible relative to the much stronger deformation downstream in the die.

- (ii) *Outlet boundary conditions*. The normal stress boundary condition and the zero radial velocity are imposed:

$$n \cdot (-p\mathbf{I} + \boldsymbol{\tau}) = -p_o, \quad v_r = 0.$$

- (iii) *Slip boundary condition at the die wall*. The Navier slip condition has been used at the die wall, which relates the slip velocity with the wall shear stress, σ_w :

$$v_s = C\sigma_w,$$

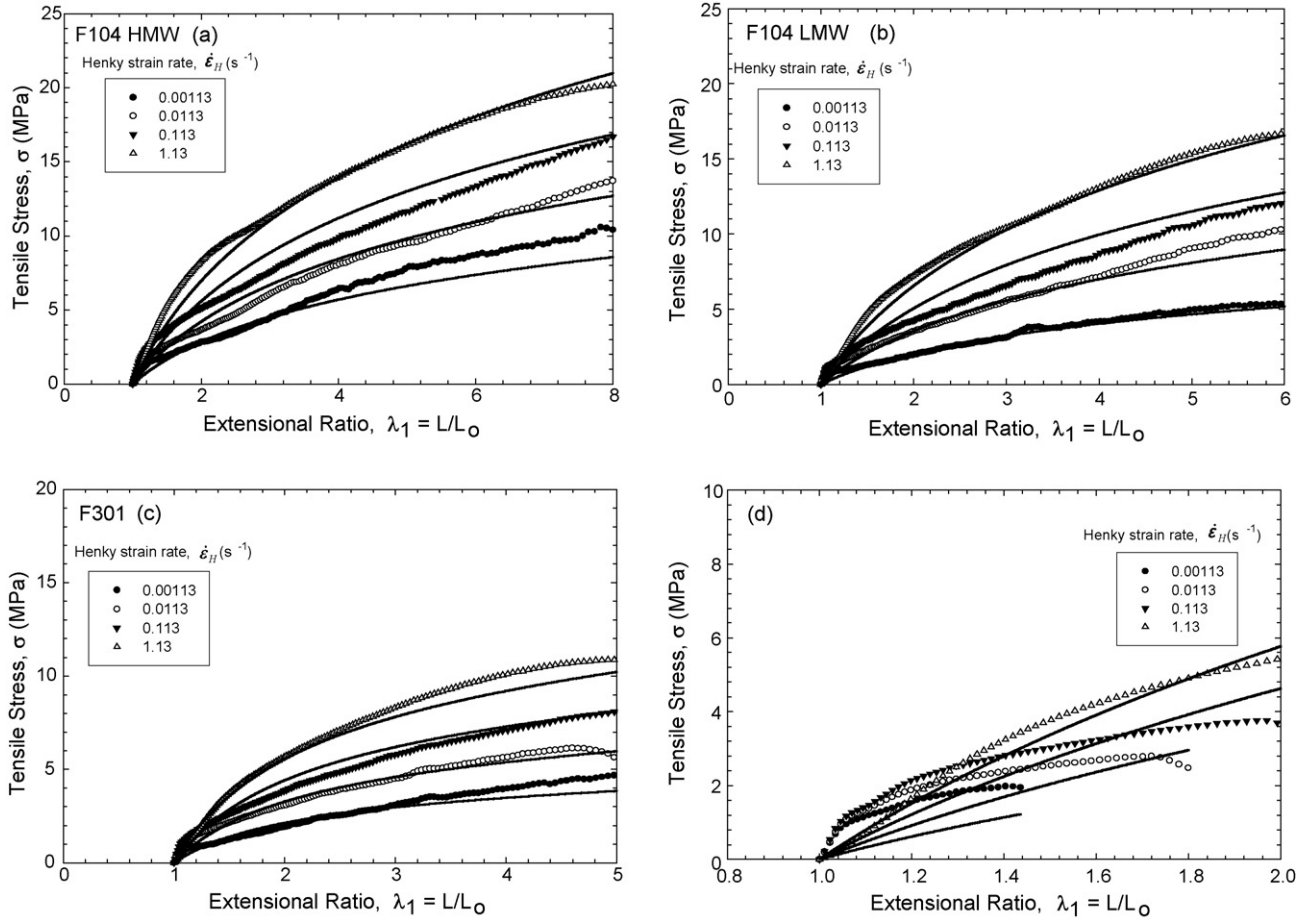


Fig. 3. (a) Uniaxial extension of F104 HMW samples stretched at different Hencky strain rates. Solid lines show fits of Eq. (15). (b) Uniaxial extension of F104 LMW samples stretched at different Hencky strain rates. Solid lines show fits of Eq. (15). (c) Uniaxial extension of F301 samples stretched at different Hencky strain rates. Solid lines show fits of Eq. (15). (d) Uniaxial extension of F303 samples stretched at different Hencky strain rates. Solid lines show fits of Eq. (15).

where $C = 1.92 \text{ m/MPa.s}$ as determined from experimental data by Patil et al. [5].

(iv) The axisymmetric boundary condition is used at $r=0$:

$$v_r = 0, \quad \frac{\partial v_z}{\partial r} = 0.$$

2.3. Finite element method

The equations of motion coupled with the proposed constitutive and structural parameter models were solved using the commercial finite element (FE) code FEMLAB 3.2 with user-defined MATLAB routines for calculating the strain history of the material and the viscoelastic stress tensor. As the problem considered here is axisymmetric, two-dimensional meshes are used on the computational domain [5]. These unstructured meshes comprise triangular elements of widely varying sizes, small and large elements being employed in regions where the rates of strain are large and small, respectively. The smallest elements are required near the die corners, especially the re-entrant corner. The total number of elements used is in the range of 3000–10,000. The corners are also rounded slightly to avoid

geometrical singularity, and the local element size is chosen to be smaller than the fillet radius at the corner. The fillet radius is a small portion of the capillary radius, and thus the solution is expected to be only slightly affected by the corner rounding.

Finite element simulations for viscoelastic flows have been done by many groups [24,25], using both differential and integral types of constitutive equations. In particular, Olley and Coates [26] and Olley et al. [27] described FE methods with ‘streamline upwinding’ elements for the K-BKZ model with strain and time damping components introduced by Papanastasiou et al. [28]. Since our constitutive model is based on the nonlinear strain tensor, time-integration along the streamlines is essential, and an approach similar to that of Olley et al. [27] has been adopted.

Since the problem is time independent, the solution involves iterations among the velocity field, the strain field, and the stress field. First, a Newtonian flow field is generated, subject to the proper boundary conditions. This trial flow field is used as a starting point of the simulation. The kinetic equation for structural parameter ξ is solved to obtain a distribution of ξ throughout the simulation domain. This will be required in the viscoelastic constitutive equation (Eq. (3)) for stress computation. Pathlines are computed based on this trial flow field to track the strain

history of fluid particles along them. Elastic stress at a point is computed by tracing back the particle path to calculate the deformation gradient tensor $\mathbf{F}(t, t')$, from which the Cauchy-Green strain tensor $\mathbf{B}(t, t')$ can be calculated. The elastic stress at that point is evaluated from Eqs. (5) and (8) using parameters listed in Table 4 for resin F104 HMW. Once these elastic stresses are computed, the total stress components are obtained by using Eqs. (3) and (4) and incorporated into the FEMLAB flow solution as a body force [27]; from this a new flow solution is obtained using the FEMLAB finite element solver. This new flow solution is then used as the new trial flow field, and the above procedure is repeated. Convergence is reached when the fractional velocity change between successive iterations is below a certain threshold (10^{-3}) over all nodes.

2.3.1. Particle tracking

The pathlines are calculated using second order time integration as described by Olley et al. [27]. Then the deformation gradient tensor $\mathbf{F}(t, t')$ is computed by integrating the following equation along the pathlines:

$$\frac{d\mathbf{F}(t, t')}{dt} = \mathbf{L}(t')\mathbf{F}(t, t'). \quad (16)$$

using a fourth-order Runge–Kutta method. $\mathbf{L}(t')$ is the velocity gradient tensor experienced by a fluid particle as it traverses the pathline. Given \mathbf{F} at a relative time, $t-t'$, the strain tensor $\mathbf{B}(t, t')$ is calculated using Eq. (5).

To validate our code, we have simulated the same contraction flow of LDPE as reported by Olley et al. [27]. The K-BKZ model with strain damping function given by Papanastasiou et al. [28] is solved for simulating the flow of LDPE melt through an abrupt 4:1 contraction. The two results are in excellent agreement. In particular, the growth of the corner vortex size with increasing apparent shear rate was successfully captured. The difference between the two solutions is below 6.8%.

The convergence of the simulation with respect to the number of elements was also confirmed. When doubling the number of mesh elements from 3000–6000, the difference in the velocity is below 3% throughout the simulation domain. The run time of the simulations is in the range of 1500–2500 s on Intel Pentium IV machines (2.8 GHz) with 1 GB RAM.

3. Result and discussion

The simulations are carried out for various die design parameters: the die reduction ratio, $RR = D_b^2/D^2$, the die land length to diameter ratio, L/D , and the die entrance angle, 2α . The simulation results are compared with the experimental data reported by Ochoa and Hatzikiriakos [14] for pastes prepared by mixing a high molecular weight PTFE (F104 HMW) with 38.8 vol.% Isopar[®] M [4].

To gain a better understanding of the structure of PTFE paste flow, typical velocity profiles at various axial locations inside the conical die ($2\alpha = 90^\circ$ and $L/D = 20$) are plotted in Fig. 4. The x -axis in Fig. 4 is the dimensionless radial distance normalized by the die radius at the corresponding axial location. The flow inside the conical section is mostly elon-

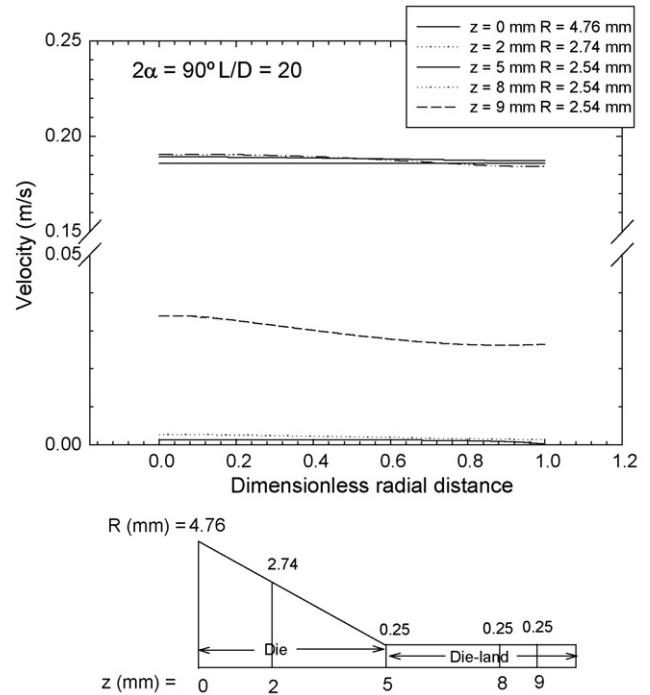


Fig. 4. Radial velocity profiles at various axial locations inside the conical die (thin lines) having an entrance angle of 90° ($\dot{\gamma}_A = 5869 \text{ s}^{-1}$, $RR = 352$) and die land (thick lines).

gational (note the significant slip at the wall) and this causes significant fibrillation (discussed below). Flow in the die land is simple shear with significant slip. Thus, the velocity profile soon attains a fully developed shape that is almost plug flow. The behavior of structural parameter ξ with operating and geometrical parameters is discussed in the section below, followed by the comparison of the simulations results with experimental observations.

3.1. Structural parameter

The structural parameter is a quantitative measure of the degree of fibrillation in the sample during extrusion. Fig. 5 shows the effect of the apparent shear rate $\dot{\gamma}_A$ ($\equiv 32Q/\pi D_b^3$) on the average structural parameter, ξ_{avg} predicted by the viscoelastic model. ξ_{avg} ($\equiv \int_0^R \xi r dr / \int_0^R r dr$) is the average over the cross section of the die at each axial position z . For small values of the apparent shear rate, ξ_{avg} increases till the exit of the conical section, which is at $z = 0.0078$ m from the inlet, and remains constant thereafter. Above a certain apparent shear rate value, $\dot{\gamma}_A \approx 55 \text{ s}^{-1}$, ξ_{avg} increases downstream and reaches a maximum some distance before the entry into the die land.

Above the apparent shear rate value of $\dot{\gamma}_A \approx 55 \text{ s}^{-1}$, the flow becomes significantly rotational just before the exit of the conical section of the die causing ψ to become negative, resulting in the maximum in the axial profile of ξ_{avg} . Then ξ_{avg} relaxes rapidly, and upon entering the die land reaches a constant level further downstream. These profiles can be explained as follows. Although the flow type is purely elongational along the axis, off the axis the flow type becomes highly rotational in the region

immediately before the end of the conical section, which is conducive to fibril breakage. For small shear rates below 55 s^{-1} , the degree of fibrillation remains low throughout, and breakage is insignificant according to Eq. (15). For higher $\dot{\gamma}_A$, ξ_{avg} and the rotational flow type cooperate to make the rate of fibril breakage higher than that of fibril creation. As a result, a maximum in the axial profile of ξ_{avg} appears, downstream of which ξ_{avg} declines. The flow in the die land is simple shear with significant slip at the wall (see velocity profiles at Fig. 4) and therefore no additional fibrils are created. Furthermore, due to significant slip at the wall, the true shear rate is small; this causes the breakage rate to become negligible. As a result, ξ_{avg} in the land region remains essentially constant. The increase in the entrance angle at a fixed shear rate causes the overall increase in the elongational rate, this leads to a higher level of ξ_{avg} throughout the die.

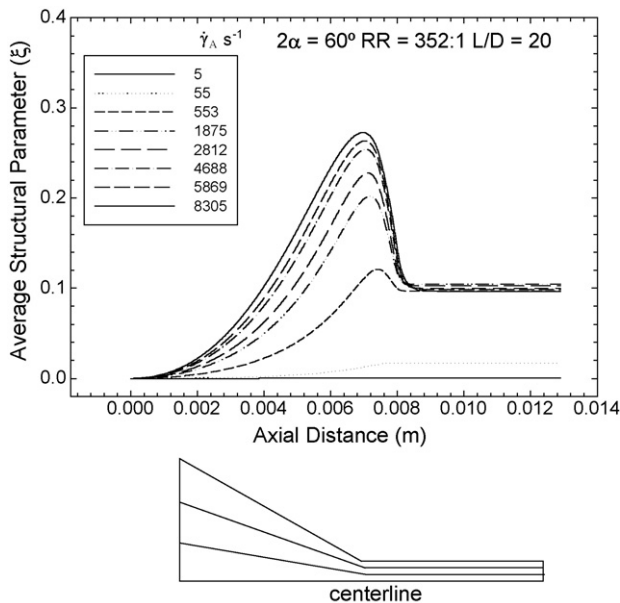


Fig. 5. Axial profiles of structural parameter along the centerline of a conical die having an entrance angle of 60° for various apparent shear rates indicated in the figure.

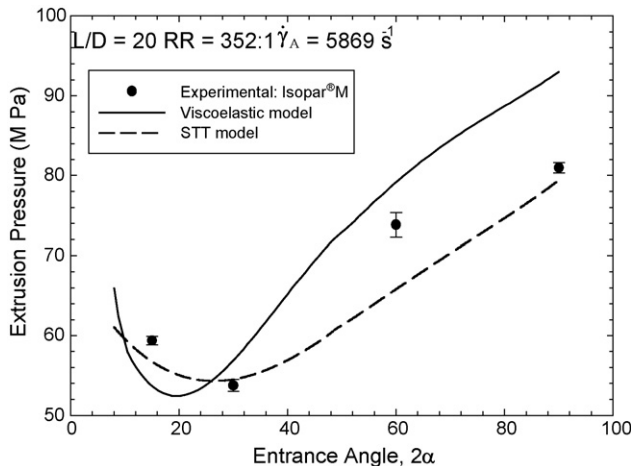


Fig. 6. The effect of die entrance angle on the extrusion pressure: comparison between experimental results and the predictions of the viscoelastic model.

3.2. Effect of die entrance angle

Simulations were performed for conical dies with $RR = 352$, $L/D = 20$ and various entrance angles in the range of $8^\circ \leq 2\alpha \leq 90^\circ$. The simulated dependence of the extrusion pressure on 2α is shown in Fig. 6. The agreement between the model predictions and experimental measurements is generally good. Also shown in Fig. 6 is the shear thinning-thickening (STT) model predictions by Pramod et al. [5], which fit the data equally well. However, the parameters of the present viscoelastic model are all determined from independent rheological experiments. There are no adjustable parameters and this makes the model a truly predictive one. In the STT model, the parameters are fitted by matching predictions directly to macroscopic quantities and thus have no direct physical meaning. This represents a key advantage of the viscoelastic model over the STT model.

The initial decrease in the extrusion pressure with the entrance angle in Fig. 6 is similar to the trend seen in capillary extrusion of polymer melts and other viscous liquids. This trend can be predicted by using the lubrication approximation assumption [11,29]. However, lubrication approximation is only valid for small entrance angles. For larger entrance angles, it would predict monotonic decrease of the extrusion pressure. In fact, the extrusion pressure of PTFE increases significantly with increase of entrance angle beyond a certain value $3\alpha \approx 30^\circ$. Such a behaviour is commonly observed in the extrusion of elastic solids; for example, see Horrobin and Nedderman [29] and the references therein.

At very small entrance angles the flow type parameter ψ is close to zero. Thus, little fibrillation takes place. The dominant contribution to the stress comes from the shear-thinning part, and the PTFE paste behaves mostly as a shear-thinning fluid. The decreasing viscosity with increasing 2α causes the initial decline in the extrusion pressure, and this is captured by the present model. As the entrance angle increases, the flow becomes more extensional and this has an impact on ψ and subsequently on ξ ,

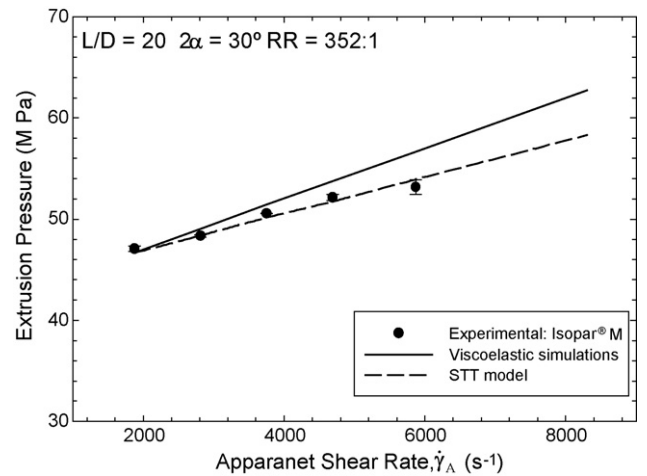


Fig. 7. The effect of apparent shear rate on the extrusion pressure of PTFE paste extrusion: comparison between experimental results and the prediction of the viscoelastic model.

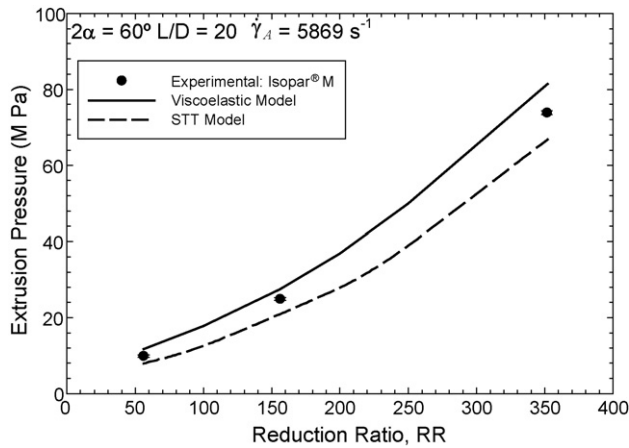


Fig. 8. The effect of the die reduction ratio, RR, on the extrusion pressure: comparison between experimental results and the predictions of the viscoelastic model.

with both dramatically increasing. The paste now becomes more solidlike and this is modelled by the elastic strain-hardening term included in the constitutive rheological model of Eq. (3). The dominant contribution at high entrance angles comes from the elastic term which causes the significant increase in the extrusion pressure.

3.3. Effect of apparent shear rate

Simulations were performed for various apparent shear rate values for a conical die having an entrance angle $2\alpha \approx 30^\circ$, $RR = 352$ and $L/D = 20$. The dependence of the extrusion pressure on the apparent shear rate, $\dot{\gamma}_A$ is shown in Fig. 7. The viscoelastic model prediction agrees well with the experimental data, and is slightly above the best fit of the STT model. The increase of the structural parameter with apparent shear rate contributes to the monotonic increase of the extrusion pressure (Fig. 7).

3.4. Effect of die reduction ratio

Simulations were performed for dies having $L/D = 20$, $2\alpha \approx 60^\circ$ and various reduction ratios in the range of $56 \leq RR \leq 352$. Fig. 8 depicts the effect of die reduction ratio on the extrusion pressure of the paste. The agreement between the numerical and experimental results is excellent. The extrusion pressure increases with the increase in the reduction ratio in a nonlinear fashion, which is captured by the simulated results. The viscoelastic prediction is again falling above the STT result.

3.5. Effect of die length-to-diameter ratio

Simulations were performed for dies with $RR = 352$, $2\alpha \approx 90^\circ$ and several L/D ratios in the range of 0–40 at an apparent shear rate of $\dot{\gamma}_A = 5869 \text{ s}^{-1}$. Fig. 9 plots the effect of L/D on the extrusion pressure of the paste. The numerical results are close to measured values for small L/D . For larger L/D , the extrusion pressure is predicted to increase linearly with the L/D ratio,

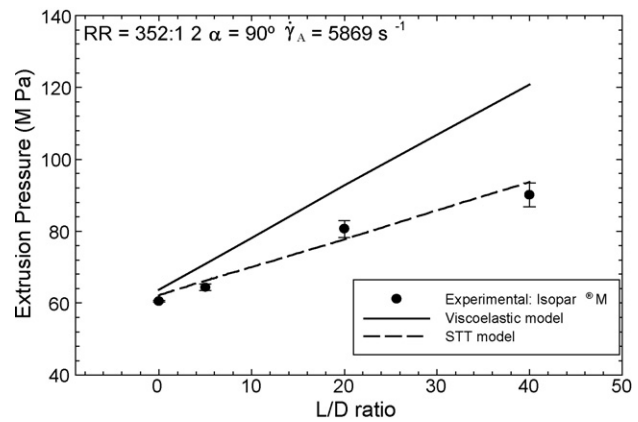


Fig. 9. The effect of length-to-diameter ratio (L/D) on the extrusion pressure: comparison between experimental results and the predictions of the viscoelastic model.

whereas the measured values tend to level off. The increasing discrepancy at larger L/D suggests that the model overpredicts the wall stress in the die land, perhaps because of the slip model used.

4. Conclusions

A viscoelastic rheological constitutive equation proposed for the paste extrusion of PTFE, with the total stress comprising a shear-thinning term and a strain-hardening term, is capable of capturing the physics of the process as previously documented by experiments [4,19,21,30]. In the absence of fibrillation, the PTFE paste is treated as a shear-thinning fluid. The creation of fibrils gradually makes the paste exhibit more elastic behaviour, and this is captured through a modified hyper-elastic Mooney–Rivlin model. Change in the nature of the paste, from a fluid-like (shear-thinning) behaviour to a solid-like (elastic) one, is implemented by the introduction of a microscopic structural parameter ξ that indicates the degree of fibrillation. A previously developed evolution equation has been used for ξ , which accounts for fibril formation and breakage based on kinetic network theories [5,12,31,32].

Simulation results were found to be in good agreement with experimental findings reported by Ochoa and Hatzikiriakos [4]. Based on this agreement it can be concluded that the proposed constitutive equation is suitable for modeling the behaviour of the paste and captures the physics of the process. The viscoelastic model proposed in this paper is a truly predictive model since its parameters are determined from independent rheological experiments.

Acknowledgements

This work has been supported financially by a grant from Daikin America. J.J. Feng acknowledges support by NSERC, Canada Foundation for Innovation and the Canada Research Chair Program. The simulations were performed on computers at the Institute of Applied Mathematics, University of British Columbia.

References

- [1] C.A. Sperati, in: J. Brandrup, E.H. Immergut (Eds.), *Physical Constants of Fluoropolymers in Polymer Handbook*, John Wiley and Sons, New York, 1989.
- [2] T.A. Blanchet, *Polytetrafluoroethylene Handbook of Thermoplastics*, Marcel Dekker Inc., New York, 1997, pp. 981–1000.
- [3] S. Ebnesajjad, *Fluoroplastics*, vol. 1. Non-Melt Processible Fluoroplastics. *Plastics Design Library*, William Andrew Corp., NY, 2000.
- [4] I. Ochoa, S.G. Hatzikiriakos, *Polytetrafluoroethylene paste preforming: viscosity and surface tension effects*, *Powder Technol.* 146 (1/2) (2004) 73–83.
- [5] P.D. Patil, J.J. Feng, S.G. Hatzikiriakos, *Constitutive modeling and flow simulation of polytetrafluoroethylene (PTFE) paste extrusion*, *J. Non-Newtonian Fluid Mech.* 139 (2006) 44–53.
- [6] S. Mazur, *Paste extrusion of poly(tetrafluoroethylene) fine powders*, in: M. Narkis, N. Rosenzweig (Eds.), *Polymer Powder Technology*, John Wiley and Sons, New York, 1995, pp. 441–481.
- [7] M. Mooney, *A theory of large elastic deformation*, *J. Appl. Phys.* 11 (1940) 582–592.
- [8] R.S. Rivlin, *Large elastic deformations of isotropic materials*, *Phil. Trans. R. Soc. Lond. Ser. A* 240 (1948) 459–490.
- [9] R.S. Rivlin, *Large elastic deformations of isotropic materials. IV. Further developments of the general theory*, *Phil. Trans. R. Soc. Lond. Ser. A* 241 (1948) 379–397.
- [10] A.F.M.S. Amin, S.I. Wiraguna, A.R. bhuiyan, Y. Okui, *Hyperelastic model for finite element analysis of natural and high damping rubbers in compression and shear*, *J. Eng. Mech.* 132 (1) (2006) 54–64.
- [11] A.P.S. Selvadurai, Q. Yu, *Constitutive modelling of a polymeric material subjected to chemical exposure*, *Int. J. Plastic.* 22 (2006) 1089–1122.
- [12] R.J. Jeyaseelan, A.J. Giacomini, *Structural network theory for a filled polymer melt in large amplitude oscillatory shear*, *Polym. Gels Networks* 3 (1995) 117–133.
- [13] P.N. Dunlap, L.G. Leal, *Dilute polystyrene solutions in extensional flows birefringence and flow modification*, *J. Non-Newtonian Fluid Mech.* 23 (1987) 5–48.
- [14] K.C. Valanis, R.F. Landel, *The strain-energy density function of a hyperelastic material in terms of the extension ratios*, *Arch. Appl. Mech.* 64 (1967) 136–146.
- [15] Y. Yamashita, S. Kawabata, *Approximated form of the strain energy density function of carbon-black filled rubbers for industrial applications*, *J. Soc. Rubber Ind. (Jpn.)* 65 (9) (1992) 517–528.
- [16] A.F.M.S. Amin, M.S. Alam, Y. Okui, *An improved hyperelastic relation in modeling viscoelasticity response of natural and high damping rubbers in compression: experiments, parameter identification, and numerical verification*, *Mech. Mater.* 34 (2002) 75–95.
- [17] S. Kawabata, H. Kawai, *Strain energy density functions of rubber vulcanizates from biaxial extension*, *Adv. Polym. Sci.* 24 (1977) 90–124.
- [18] A. Yoshimura, R.K. Prud'Homme, *Wall slip corrections for coquette and parallel disk viscometers*, *J. Rheol.* 32 (1) (1988) 53–67.
- [19] I. Ochoa, *Paste extrusion of polytetrafluoroethylene fine powder resins: the effects of the processing aid physical properties*, Ph.D. Dissertation, The University of British Columbia, Department of Chemical and Biological Engineering, 2006.
- [20] M.L. Sentmanat, *A novel device for characterizing polymer flows in uniaxial extension*, in: *SPE, ANTEC Proceedings*, 2003, pp. 992–996.
- [21] A.B. Ariawan, S. Ebnesajjad, S.G. Hatzikiriakos, *Paste extrusion of polytetrafluoroethylene (PTFE) fine powder resins*, *Can. J. Chem. Eng.* 80 (2002) 1153–1165.
- [22] G.G. Fuller, J.M. Rallison, R.L. Schmidt, L.G. Leal, *The measurements of velocity gradients in laminar flow by homodyne light-scattering spectroscopy*, *J. Fluid Mech.* 100 (3) (1980) 555–575.
- [23] G.G. Fuller, L.G. Leal, *Flow birefringence of dilute polymer solutions in two-dimensional flows*, *Rheol. Acta* 19 (1980) 580–600.
- [24] M.J. Crochet, A.R. Davies, K. Walter, *Numerical Simulation of Non-Newtonian Flow*, Elsevier, Amsterdam, 1984.
- [25] R.G. Owens, T.N. Phillips, *Computational Rheology*, Imperial College Press, London, 2002.
- [26] P. Olley, P.D. Coates, *An approximation to the KBKZ constitutive equation*, *J. Non-Newtonian Fluid Mech.* 69 (1997) 239–254.
- [27] P. Olley, R. Spires, P.D. Coates, *A method for implementing time-integral constitutive equations in commercial CFD packages*, *J. Non-Newtonian Fluid Mech.* 86 (1999) 337–357.
- [28] A.C. Papanastasiou, L.E. Scriven, C.W. Macosko, *An integral constitutive equation for mixed flows: viscoelastic characterization*, *J. Rheol.* 27 (1983) 387–410.
- [29] D.J. Horrobin, N.R. Nedderman, *Die entry pressure drops in paste extrusion*, *Chem. Eng. Sci.* 53 (1998) 3215–3225.
- [30] A.B. Ariawan, *Paste extrusion of polytetrafluoroethylene fine powder resins*, Ph.D., The University of British Columbia, Department of Chemical and Biological Engineering, 2002.
- [31] T.Y. Liu, D.S. Soong, M.C. Williams, *Transient and steady rheology of polydisperse entangled melts: predictions of a kinetic network model and data comparisons*, *J. Polym. Sci.: Pl. Phys. Ed.* 22 (1984) 1561–1587.
- [32] S.G. Hatzikiriakos, D. Vlassopoulos, *Brownian dynamics simulations of shear-thickening in dilute polymer solutions*, *Rheol. Acta* 35 (1996) 274–287.